

The Complex Wind Torus and Jets of PSR B1706–44

Roger W. Romani¹, C.-Y. Ng¹, Richard Dodson² & Walter Brisken³

¹*Department of Physics, Stanford University, Stanford, CA 94305*

²*The Institute of Space and Astronautical Science, 3-1-1 Yoshinodai, Sagamihara, Kanagawa 229-8510, Japan*

³*National Radio Astronomy Observatory, P.O. Box O, Socorro, NM 87801*

rwr@astro.stanford.edu, ncy@astro.stanford.edu, rdodson@vsop.isas.jaxa.jp,
wbrisken@aoc.nrao.edu

ABSTRACT

We report on *Chandra* ACIS imaging of the pulsar wind nebula (PWN) of the young Vela-like PSR B1706–44, which shows the now common pattern of an equatorial wind and polar jets. The structure is particularly rich, showing a relativistically boosted termination shock, jets with strong confinement, a surrounding radio/X-ray PWN and evidence for a quasi-static ‘bubble nebula’. The structures trace the pulsar spin geometry and illuminate its possible relation to SNR G343.1–2.3. We also obtain improved estimates of the pulsar flux and nebular spectrum, constraining the system age and energetics.

Subject headings: gamma rays: observations, stars: pulsars: individual B1706–44

1. Introduction

PSR B1706–44, discovered by Johnston et al. (1992) is among the most interesting pulsars for study at high energies. It is one of a handful of pulsars detected by EGRET in GeV γ -rays. It is quite similar to the Vela pulsar with a characteristic age $\tau_c = P/(2\dot{P}) = 1.7 \times 10^4$ yr and a spindown luminosity of $\dot{E} \approx 4 \times 10^{36}$ erg/s, but is $\sim 10\times$ more distant at $d = 3d_3$ kpc. Early *Chandra* HRC/ACIS data provided a first detection of X-ray pulsations and showed a compact $\sim 10''$ surrounding pulsar wind nebula (PWN) (Gotthelf, Halpern, & Dodson 2002; Dodson & Golap 2002). More recent *XMM-Newton* spectroscopy (McGowan et al. 2004) has provided improved measurements of the X-ray spectrum and pulsations. Early claims that the PWN is detected in TeV γ -rays (Kifune et al. 1995; Chadwick et al. 1997) have not been supported by recent HESS observations (Aharonian et al. 2005).

PSR B1706–44 is superposed on a radio-bright spur of the supernova remnant G343.1–2.3, which has a similar, albeit unreliable, $\Sigma - D$ distance of ~ 3 kpc (McAdam, Osborne & Parkinson 1993). The pulsar DM gives a distance of 2.3 ± 0.3 kpc in the Cordes & Lazio (2002) model. Dodson & Golap (2002) have argued for an association. In particular, they found a faint southern extension of the SNR, which would place the pulsar within the full SNR boundary. They also noted an approximately N-S elongation of the X-ray PWN, pointing roughly back to the SNR center and argued that this would represent a trailed nebula. The required velocity for travel from the approximate geometric center of the SNR, about $12'$ away, was $\sim 1000d_3/\tau_4$ km/s where τ_4 is the pulsar age in units of 10^4 yr. There are, however, some challenges to this SNR association. Koribalski et al. (1995) in an HI absorption study of the pulsar found velocity components setting lower and upper bounds

for the distance of $d_{min} = 2.4 \pm 0.6$ kpc and $d_{max} = 3.2 \pm 0.4$ kpc. However a prominent HI emission feature seen in the bright limb of G343.1–2.3 at -32 km/s is not seen by Koribalski et al. in the absorption spectrum of the pulsar, suggesting that it lies in front of the SNR. Also scintillation studies (Nicastrò, Johnston & Koribalski 1996; Johnston, Nicastrò & Koribalski 1998) suggest a low transverse velocity for the pulsar, $v \leq 89$ km/s. This estimate has been supported by more recent scintillation measurements (Johnston, priv. comm). Thus the distances of the pulsar and SNR are still fairly uncertain. We adopt here a generic distance of 3 kpc in the discussion that follows, but carry through the scaling to show the distance dependence.

Ng & Romani (2004) re-examined the AO1 50 ks HRC and ~ 15 ks ACIS-S exposures, and found that the compact PWN could be well modeled as an equatorial torus + polar jets, rather similar to the structures seen around the young Crab and Vela pulsars. They found that the brightest arc of PWN emission lay *behind* the pulsar’s inferred motion from the SNR center, while a polar jet extended well in front of the pulsar position. This is difficult to reconcile with a bow shock/trail interpretation. On the other hand, the PWN symmetry axis did indeed point back to the SNR center, suggesting that a more careful evaluation of the connection was in order. This is particularly interesting, since comparison of the PWN symmetry (= pulsar spin) and proper motion axes can constrain the origin of pulsar birth kicks (Spruit & Phinney 1998; Lai, Chernoff & Cordes 2001; Romani 2004).

We have obtained a deeper 100 ks ACIS-I exposure of PSR B1706–44 and surroundings. The X-ray exposure coverage is compared to the overall geometry of G343.1–2.3 in Figure 1. Together with new ATCA radio continuum imaging we are able to study the rich structure in this PWN and further constrain its connections with the SNR.

2. Observations and Data Analysis

PSR B1706–44 was observed with the *Chandra* ACIS-I array (4 ACIS-I chips along with the S3 and S4 chips) on February 1-2, 2004 with standard imaging (3.2s TE) exposures. The CCD array was operated in ‘very faint’ (VF) mode, allowing improved rejection of particle backgrounds. The total live-time was 98.8 ks and no episodes of strong background flaring were observed. Hence all data are included in our analysis. The pulsar was positioned near the standard aimpoint of the I3 chip and all observing conditions were normal. We have also compared our new exposure with the archival (February 3, 2001) 14.3 ks ACIS-S3 exposure (obsID 0757). As usual the backside illuminated S3 chip suffered more from particle background and after cutting out periods of background flares, 11 ks of clean exposure remained. All analysis was performed using CIAO 3.2 and CALDB 3.0.0, including automatic correction for the ACIS QE degradation. These data were nearly free of pile-up; the maximum pixel counts at the pulsar position indicate only 2.5% pile-up while the best fit model for the point source has an expected pile up fraction of $\sim 3.5\%$. For sources with low pile-up we can maximize the spatial resolution of the ACIS image by removing the standard pixel randomization and applying an algorithm correcting the position of split pixel events (Mori et al. 2001). This decreases the on-axis PSF width in our data set by $\gtrsim 10\%$. These data are compared with radio observations of the PWN.

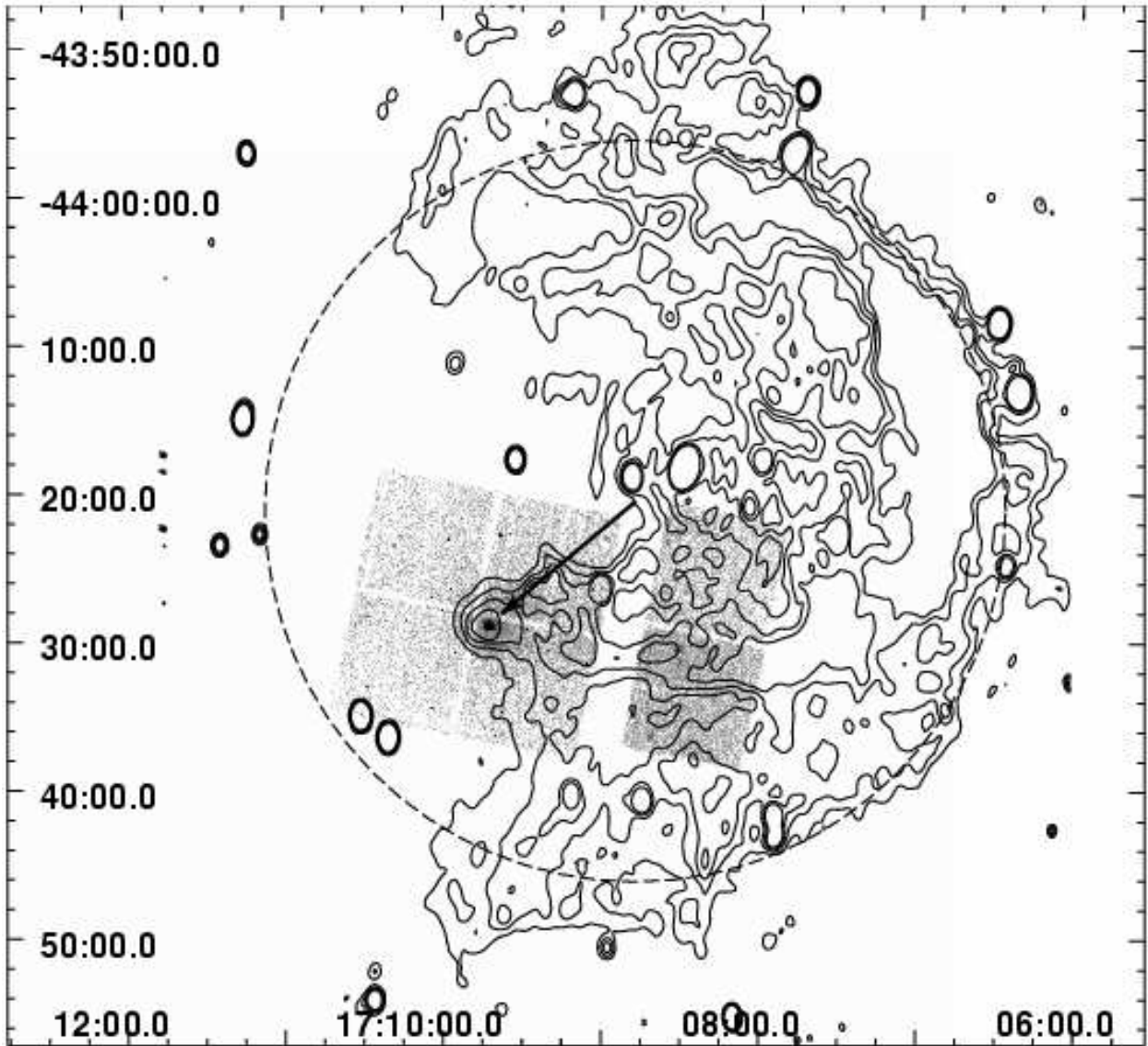


Fig. 1.— Greyscale image of our new ACIS-I pointing of PSR B1706–44. The contours (at 8, 10, 12 and 14 mJy/beam) show the shell of G343.1–2.3 from a 19 pointing 1384 MHz ATCA mosaic (Dodson & Golap 2002). The radio map has a resolution of $70'' \times 47''$ and an rms final map noise of 0.6 mJy. The X-ray PWN lies on a spur of radio emission. An approximate boundary of the full SNR ($25'$ radius) and an arrow for the inferred PSR motion, assuming birth at the SNR center, are shown.

2.1. Radio Imaging and Astrometry

Data for the radio maps shown here were collected at the Australia Telescope Compact Array (ATCA) in Narrabri (latitude -30.3°) (Frater, Brooks & Whiteoak 1992). For the 1.4 GHz map in Figures 1 and 2a, the data acquisition and analysis are described in Dodson & Golap (2002). For the image contours in Figure 3a, the data first presented in Dodson & Golap (2002) were re-imaged including the 6 km baselines

and uniform weighting to highlight the high resolution features. The restoring beam size is $9''.0 \times 7''.8$. To show the nebular structure, an 11mJy point source PSF has been subtracted at the position of the pulsar. Two maxima appear flanking the pulsar position. These are unlikely to be artifacts due to pulsar variability, as diffractive scintillation for this pulsar is particularly weak (Johnston, Nicastro & Koribalski 1998). Since the data were collected in five sessions, spread over more than a year, it is in principal possible for slow refractive scintillation to change the pulsar flux between epochs and distort its PSF. However, each epoch used ~ 12 h of integration, so any residual epoch PSF should be close to circularly symmetric, in contrast to the structure near the pulsar which is clearly bipolar. Further observations, with pulsar binning, have been requested to confirm this result.

For the 4.8GHz map in Figure 2b, observations were made at 4.8- and 8.6GHz with the array in the standard configurations 0.75A, 1.5A and 6A on 06 Jan, 16 Feb and 11 Apr 2002. The maximum and minimum baselines for the 4.8-GHz data were 1 and 100 k λ (angular resolutions of $3.4'$ to $2''.1$) for a total of 26 hours observation. In all cases we observed the two frequencies with bandwidths of 128 MHz. We used the ATNF correlator mode that divides each integration's data into separate phase bins spanning the pulsar period. This firstly allowed the strongly pulsed point source flux to be excluded from the image and secondly allowed us to self-calibrate using the relatively strong point source flux from the pulsar. After data editing and calibrating we inverted the image with a uv -taper of $20''$ and deconvolved it with the full polarization maximum entropy task PMOSMEM in MIRIAD.

The most important test of the SNR association would, of course, be a direct astrometric proper motion. With a 1.4GHz flux of ~ 11 mJy, PSR B1706–44 is relatively bright. As such it is suitable for phase referenced VLBI astrometry, if an in-beam reference could be found. Unfortunately searches for phase references adequate for Australian Long Baseline Array (LBA) and US VLBA experiments have not detected comparison sources with compact fluxes greater than ~ 1 mJy. Attempts were made at external phase reference VLBA astrometry. However at 1.4GHz, the nearest known reference source (2.5° away) was scatter broadened to ~ 50 mas. With the strong ionosphere at such low elevation, the next nearest known source (10° away) is too distant for effective calibration. Since the pulsar spectrum is steep, an attempt at VLBA astrometry at 5GHz was also unsuccessful; at this low elevation the system temperature was $4 - 5 \times$ nominal and only six VLBA antennae could be used, reducing the sensitivity to $\sim 15\%$ of nominal. So unfortunately we have only tied-array astrometry at present. Even if the pulsar does travel from the geometric center of G343.1–2.3, the expected proper motion is only ~ 40 mas/yr; the existing time base of VLA/ATCA imaging does not yet allow a serious constraint on this motion. We must conclude that a direct proper motion measurement awaits substantially increased (SKA or EVLA) capabilities and a long-duration, large base-line experiment.

2.2. X-ray Spatial Analysis

To show the diffuse emission surrounding PSR B1706–44 we plot (Fig. 2a) a 1-7keV image with point sources removed (except the pulsar). These data are exposure corrected to minimize the chip gaps and heavily smoothed on a $20''$ scale. The diffuse emission is an edge-brightened, radius $\sim 110''$ cavity surrounding the pulsar with a faint extension to the west. Contours of the 1.38GHz radio map show good correlation with the radio emission in the bar crossing G343.1–2.3 (Fig. 1). We will refer to this structure as the ‘nebula’.

Moving in toward smaller scale, in 2b we show a 1-7keV image, smoothed with a $1''.5$ Gaussian. Point sources have not been removed. This shows that the cross structure fit by Ng & Romani (2004) extends

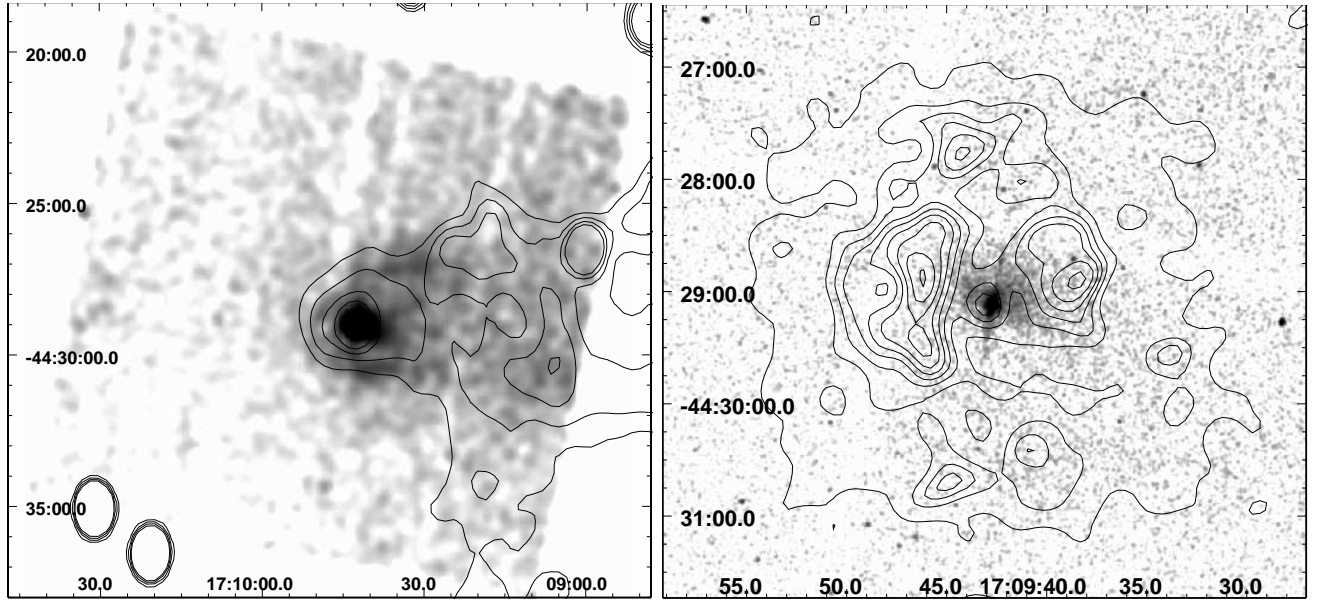


Fig. 2.— Left: ACIS-I 1-7 keV image with point sources (other than the pulsar) removed, exposure correction and $20''$ Gaussian kernel smoothing. Contours are from the 1.38 GHz radio map of Figure 1. Right: $1''.5$ Gaussian smoothed image of the PWN with an overlay of the core of the radio nebula from a 4.8 GHz ATCA image (contours at 0.4, 0.8, 1.0, 1.1,...1.6 mJy/beam); the resolution is $20''$ and the image RMS is 0.2mJy/beam.

across $\sim 1'$. Narrow X-ray jets, which we refer to here as the ‘outer jet’ (extending south) and ‘outer counter jet’ (extending north) start $\sim 10''$ from the pulsar and continue to $\sim 30''$. Bracketing these is faint diffuse X-ray emission which we will call the ‘equatorial PWN’. For comparison we draw contours of a 4.8 GHz ATCA image with $21'' \times 18''$ restoring beam. These observations have the pulsar ‘gated out’ and show that the radio PWN has a hollow center bracketing the equatorial PWN. Diffuse radio peaks are, in fact, seen just east and west of this X-ray structure.

Finally, we show in Figure 3 a lightly smoothed image of the central region of the PWN, stretched to bring out the faint outer jets. The contours are drawn from a 1.38 GHz ATCA image, where the 6-km baselines have been weighted to produce a $9''.0 \times 7''.8$ restoring beam. A point source PSF has been subtracted at the pulsar position. Two local radio maxima with peak fluxes ~ 2 mJy and ~ 2.5 mJy bracket the ‘torus’ structure. The radio then shows a sub-luminous zone surrounding the ‘equatorial PWN’; beyond $\sim 30''$ the radio brightens again, as in figure 2b. No emission appears along the ‘outer jets’. Indeed there appear to be evacuated channels in the radio emission, but improved S/N and resolution are needed to probe this sub-mJy structure. The frames on the right show the innermost region of the PWN with the best-fit torus + inner jet model (§2.3).

The overall geometry of the PWN is strongly reminiscent of that surrounding the Vela pulsar. In particular Pavlov et al. (2003) have described a series of ACIS images of the Vela nebula which show a torus-like structure, an inner jet and counter jet and a faint narrow outer jet system. This imaging sequence showed that the Vela outer jet, which is patchy and strongly bent, varies dramatically on timescales of days to weeks. Apparent motion of blobs within the jets suggests mildly relativistic bulk velocities and strong

instabilities. For PSR B1706–44 our single sensitive image does not let us comment on variability. However we argue that the relatively straight and narrow jets, $\sim 3\times$ longer than those of Vela, and symmetric PWN structure are a consequence of a static uniform external environment and a low pulsar velocity. At 1.4–8.5 GHz Dodson et al. (2003) have found that the Vela PWN has two bright patches bracketing the X-ray torus and jets, in a structure quite similar to that in Figure 2b. Polarization imaging of the Vela radio structure suggests that these two patches represent the limbs of a toroidal B field structure. This implies that the rotation axis controls the PWN symmetry to large radii.

2.3. Nebula Structure Fits

Following Ng & Romani (2004) we have fitted our new ACIS image to a point source PSF, Doppler boosted equatorial torus, polar jets and uniform background. The fitting minimizes residuals using a Poisson-based likelihood function. Monte Carlo simulations of Poisson realizations of the best-fit model are in turn re-fitted to generate statistical errors and their co-variance matrices. Table 1 contains the best-fit values. The torus radius and axis inclination and position angles are r , ζ and Ψ , respectively. See Ng & Romani (2004) for the definition of the other parameters and the details of the fitting technique. In Table 1 the inner jet/counter-jet are constrained to lie along the torus axis in the fits.

In addition to the statistical errors, there are certainly systematic errors, in particular induced by

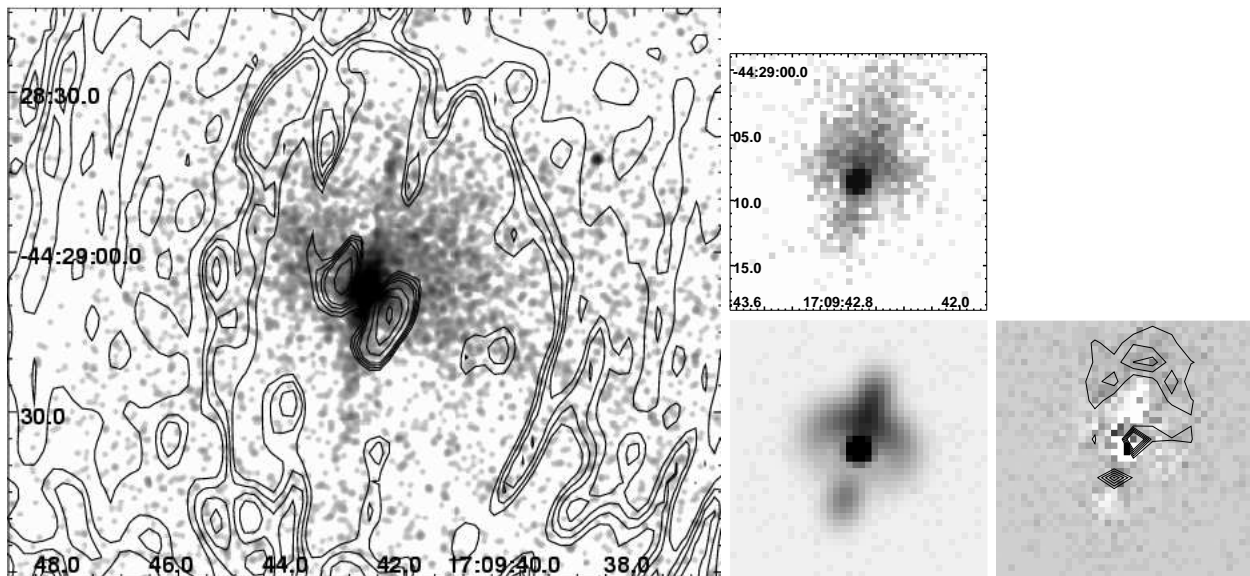


Fig. 3.— Left: Grey scale image ($1''.5$ Gaussian smoothing) of the PWN, stretched to show the outer jets and the equatorial PWN. The contours (0.3, 0.4, 0.5, 0.6, 0.9, 1.2, 1.5 mJy/beam) are from the 1.38 GHz ATCA image, which has a map rms of 0.2 mJy/beam and a resolution of $9''.0 \times 7''.8$. The pulsar point source has been subtracted. Two peaks of radio emission bracket the torus. These lie in a cavity which surrounds the equatorial PWN and jets. Middle: grey scale image of the inner PWN (above) and of the best-fit point source+torus+(inner)jets model (Table 1) to the same scale(below). At the far right, the residual image is shown, with contours indicating the excess counts above (North of) the torus.

Table 1: Torus Fit Parameters with 1σ Statistical Errors

| Ψ (deg) | ζ (deg) | r (arcsec) | δ | β | Point Source [†] | Torus [†] | Jet [†] | Counter-jet [†] |
|-----------------|----------------------|-----------------------|----------|-----------------|---------------------------|--------------------|------------------|--------------------------|
| 163.6 ± 0.7 | $53.3^{+1.6}_{-1.4}$ | $3.3^{+0.08}_{-0.06}$ | 1.0* | 0.70 ± 0.01 | 2897^{+65}_{-52} | 1221^{+55}_{-41} | 185^{+8}_{-21} | 325^{+43}_{-54} |

* – held fixed † counts

unmodeled PWN components. For example, it is clear that there are counts in excess of the torus+jet model in a cap surrounding the inner counter-jet. Interestingly similar structure is seen in the Crab PWN. We have made an attempt to constrain the systematic biases by modifying the fitting model. For example, allowing the (inner) jet and counter-jet to have a free position and amplitude shifts the best-fit position angle to $\Psi = 165 \pm 0.5^\circ$ and the inclination to $\zeta = 56.7 \pm 1.0^\circ$. We therefore infer systematic errors about $3\times$ larger than our rather small statistical errors.

We have also measured the outer jet/counter-jet system. Minimizing the residual to a 1-D line passing through the pulsar, the two jets together lie at $\Psi_{\text{outer}} = 169.4 \pm 0.15^\circ$. If the jets are fitted separately, we obtain $\Psi_{\text{outer}} = 168.4 \pm 0.2^\circ$ and $170.9 \pm 0.2^\circ$ for the outer jet and counter-jet, respectively. Thus the two jets are mis-aligned at the $\sim 8\sigma$ level. A fit to the count distribution about the best fit axis shows that the narrow outer counter-jet has a Gaussian FWHM across the jet of $2''.3 \pm 0''.2$. The outer jet appears broader at the base with an initial width of $4''.9 \pm 0''.5$, continuing at FWHM= $2''.7 \pm 0''.3$ for its outer half. These estimates have been corrected for the telescope PSF, which is quite uniform this close to the aimpoint.

It is important to note that at the observation roll angle, the read-out direction lies at $\Psi = 168.7^\circ$! Due consideration, however, shows that the jet structure cannot be produced by the read-out trail. First the jets cover only $\sim 1'$; the read-out excess should cover the full I3 chip. Second the pulsar provides only ~ 2900 1–7 keV counts. The read-out trail (out-of-time) image of this source should contribute only 36 counts over the full $8.3'$ strip across I3 and ~ 2.5 counts in the ‘jet regions’; the outer jet and counter-jet have 92 and 93 1–7 keV counts, respectively. Finally the outer jets are much harder than the soft X-ray emission from the pulsar; indeed with a mean detected photon energy ~ 2 keV these are the hardest extended features in the image.

The over-all system, showing an asymmetric torus, broad inner jets and narrow outer jets is, of course, very similar to the Vela PWN as studied with *Chandra* by Pavlov et al. (2003). We will discuss the comparison with the Vela system in §3, highlighting the differences. We interpret these as suggesting that the PSR B1706–44 PWN has developed from a low velocity pulsar.

2.4. Spectral Analysis

For the best possible constraints on the source spectrum, we have reprocessed both the ~ 11 ks cleaned ACIS-S data set and our new ~ 100 ks ACIS-I data set with the new time-dependent gain adjustment and CTI correction available in CIAO 3.2. The updated RMFs should in particular improve the low energy calibration, important for obtaining the best estimates of N_H . As noted above, in these data sets the pile-up was negligible at $\sim 3\%$. To model the aperture corrections, 10 PSFs with monochromatic energies from 0.5 to 9.5 keV were simulated using the Chandra Ray-Tracer program, ChaRT. The enclosed energy fraction as a function of radius was fitted to a linear function of energy and this was used to correct the ARFs used in the spectral fit. In extracting the pulsar spectrum, an aperture of radius $1''$ was used to minimize nebular contamination. Results from the combined fits of the ACIS-I and ACIS-S pulsar data sets are listed in

Table 1; the spectral fits are substantially better for composite models with both thermal and power-law components. Spectral parameter errors are projected multi-dimensional 1σ values. We quote both absorbed and unabsorbed fluxes. As is often the case with low statistics X-ray spectra, projected (multi-dimensional) errors on the fluxes are very large due to spectral parameter uncertainties. Thus, we follow other authors in quoting flux errors as 1σ single parameter values.

Table 2: Spectral Fits to PSR B1706–44

| Model | N_H 10^{21}cm^{-2} | Γ | abs.flux $f_{0.5-8}^\dagger$ | unabs. flux $f_{0.5-8}^\dagger$ | T^∞ MK | R^∞ km | abs. flux $f_{0.5-8}^\dagger$ | unabs. flux $f_{0.5-8}^\dagger$ | χ^2/dof |
|--------|----------------------------------|------------------------|---------------------------------|------------------------------------|------------------------|-----------------------|----------------------------------|------------------------------------|---------------------|
| PL | 3.8 ± 0.3 | $3.06^{+0.15}_{-0.14}$ | 2.01 ± 0.04 | 4.74 ± 0.1 | - | - | - | - | 145.9/99 |
| BB | 1.0 ± 0.3 | - | - | - | 3.7 ± 0.2 | $0.4^{+0.13}_{-0.11}$ | 1.42 ± 0.03 | 1.76 ± 0.04 | 288.4/99 |
| PL+BB | $4.7^{+0.8}_{-0.7}$ | 1.62 ± 0.2 | 1.70 ± 0.07 | 2.25 ± 0.1 | $2.00^{+0.17}_{-0.16}$ | $2.4^{+1.6}_{-1.0}$ | 0.83 ± 0.03 | 3.85 ± 0.12 | 40.6/97 |
| | 5.0^* | 1.68 ± 0.17 | 1.70 ± 0.07 | 2.33 ± 0.1 | 1.93 ± 0.06 | $2.8^{+0.76}_{-0.70}$ | 0.82 ± 0.03 | 4.40 ± 0.14 | 40.8/98 |
| PL+Atm | $5.9^{+0.9}_{-0.8}$ | 1.67 ± 0.2 | 1.67 ± 0.07 | 2.34 ± 0.1 | $0.79^{+0.13}_{-0.11}$ | 13.1^* | 0.85 ± 0.03 | 6.8 ± 0.2 | 40.7/97 |
| | 5.0^* | 1.56 ± 0.17 | 1.67 ± 0.07 | 2.2 ± 0.1 | 0.91 ± 0.05 | 13.1^* | 0.88 ± 0.03 | 4.92 ± 0.15 | 40.8/98 |

\dagger 0.5-8 keV fluxes in units of $10^{-13}\text{erg}/\text{cm}^2/\text{s}$ * held fixed

To get the best constraints on the point source spectrum, Table 2 gives fits with N_H held to the value from the power law fits to the extended emission. We have also compared our results with the *XMM-Newton* fitting of McGowan et al. (2004), by fitting counts in the $20''$ aperture used in that observation. Our parameters and fluxes for the thermal component are generally in very good agreement. However, since this aperture contains much of the torus and central PWN, *XMM-Newton* substantially overestimates the non-thermal flux for the point source. Their fit power law flux corresponds to $7.5 \times 10^{-13}\text{erg}/\text{cm}^2/\text{s}$ (0.5-8keV, unabsorbed). In the $20''$ aperture we find $9.6 \times 10^{-13}\text{erg}/\text{cm}^2/\text{s}$ (0.5-8keV); while the small *Chandra* point source aperture gives $2.3 \times 10^{-13}\text{erg}/\text{cm}^2/\text{s}$ (0.5-8keV) for the power law component. We find a similar $\sim 3\times$ excess in the power-law + atmosphere flux for the fit to the large *XMM-Newton* aperture. Conversion of the power law flux observed in our small point source aperture to the *XMM-Newton* band shows that the expected PN+MOS (0.2-10 keV) count rate is 18% of the total (power law + thermal) counts in the $20''$ aperture. In soft (0.2-1.35 keV) and hard (1.35-10 keV) bands the predicted fraction of the counts from the power law are 12% and 21%, respectively. However the light curves of McGowan et al. (2004) show that the pulse fractions are 21% (soft), 12% (hard) and 11% (total). Since the small aperture power law produces only 12% of the soft counts but 21% are pulsed, there must a thermal pulse component. Conversely, since the power law produces 21% of the hard band flux, but this only has a pulse fraction of 12%, some of the power law counts must be unpulsed. Extrapolation of the PWN count excess above the point source PSF in the sub-luminous zone at $2-3''$ produces $\lesssim 1\%$ of the point source aperture counts. Thus the larger scale torus emission does not contribute significantly to the point source power law and cannot account for its unpulsed component. This suggests that part of the magnetospheric emission is nearly isotropic or that there is a very compact ($\lesssim 1''$) PWN component at the pulsar position.

For the thermal component, the fit flux gives an emitting area (effective radius) as a function of distance. Our fit to a pure blackbody gives $R_{eff} = 2.8d_3$ km. Thus for reasonable distances, this flux represents hot $T \sim 2 \times 10^6$ K emission from a small fraction of the stellar surface ($\sim 4.5\%$ for an $R^\infty = 13.1$ km star). The light element neutron star atmosphere models, such as the pure H 10^{12} G model grid used here (Zavlin et al. 1996), have large Wien excesses. When fit they give lower T_{eff} . Also, the black body departures allow one, in principle, to fit both the surface redshift and radius. In practice, these are typically highly degenerate in CCD-quality data. We assume here a generic surface radius of $R_s = 10$ km, corresponding to $R_\infty = R_s(1 - 2GM/R_sc^2)^{-1/2} = 13.1$ km. With N_H free (giving $5.9 \pm 0.9 \times 10^{21}\text{cm}^{-2}$) our thermal flux normalization gives a radiating radius of $R_\infty = 27.4d_3$ km, which is difficult to reconcile with expected neutron star radii for any $d > 1.8$ kpc. However, when N_H is fixed at the nebular value of $5 \times 10^{21}\text{cm}^{-2}$, we

get an effective radius of $R_\infty = 16.1d_3\text{km}$, which is tolerable even at our nominal 3 kpc distance.

Analysis of the low signal-to-noise, extended flux depends critically on the background subtraction. Given the limited statistics, only simple absorbed power-law fits were attempted for all non-thermal sources. The results are listed in Table 3. For consistency, all fits are to the 0.5-8 keV range and we quote both absorbed and unabsorbed fluxes.

Table 3: Spectral fits to extended sources

| Object | N_H 10^{21}cm^{-2} | Γ | abs. flux $f_{0.5-8}^\dagger$ | unabs. flux $f_{0.5-8}^\dagger$ | χ^2/dof |
|----------------|----------------------------------|------------------------|----------------------------------|------------------------------------|---------------------|
| Nebula | $5.0 \pm 0.4^\ddagger$ | $1.77_{-0.08}^{+0.09}$ | 5.6 ± 0.23 | 7.9 ± 0.32 | 67.4/77 |
| Equatorial PWN | $5.0 \pm 0.4^\ddagger$ | 1.57 ± 0.08 | 2.4 ± 0.07 | 3.2 ± 0.09 | 70.3/81 |
| Torus | $5.0 \pm 0.4^\ddagger$ | 1.48 ± 0.08 | 1.5 ± 0.05 | 1.9 ± 0.07 | 39.8/53 |
| Jet | 5.0^* | $1.26_{-0.13}^{+0.14}$ | 0.42 ± 0.03 | 0.52 ± 0.04 | 12.0/18 |
| Counter Jet | 5.0^* | 1.39 ± 0.10 | 0.81 ± 0.04 | 1.0 ± 0.05 | 10.8/18 |
| Outer Jets | 5.0^* | 1.26 ± 0.18 | 0.27 ± 0.03 | 0.33 ± 0.03 | 11.9/18 |

† 0.5-8 keV fluxes in units of $10^{-13}\text{erg}/\text{cm}^2/\text{s}$ * held fixed ‡ Simultaneous N_H fit.

Note that there is significant softening of the extended emission as one progresses to larger scales and that the jet components appear to be the hardest of all. This is certainly consistent with the idea that the central pulsar supplies fresh energetic electrons and that synchrotron burn-off increasingly softens the spectrum as older populations are viewed in the outer PWN. Again this trend is common in the well-measured young PWNe. Allowing the photon index to vary for the different nebula components, the best fit to a global absorption value for the extended emission gives us our fiducial $N_H = 5 \times 10^{21}\text{cm}^{-2}$. This is consistent with free-fit values for the point source, but given complexities of the composite thermal+power law model, we consider the nebular fit value more robust. Note that with $\text{DM}=75.7\text{ cm}^{-3}\text{pc}$, the $H/n_e \approx 21$ for this sight-line is large, but not unprecedented for low $|b|$ pulsars. This is also consistent with the H_I absorption measurements and a fiducial SNR distance $\sim 3\text{ kpc}$, given the appreciable uncertainties.

3. Interpretation and Conclusions

A number of authors have discussed the evolution of a PWN within an expanding supernova remnant. For example, van der Swaluw (2001) and Chevalier (2005) describe the early evolution when the supernova ejecta are in free expansion. Later, after the remnant interior is heated by the passage of the reverse shock, the PWN evolves within the Sedov phase supernova remnant whose radius is $R_{\text{SNR}} = 1.17(E_0/\rho)^{1/5}t^{2/5}$ for an explosion energy E_0 in a $\gamma = 5/3$ medium of density ρ . PSR B1706–44 has a characteristic age $10^4\tau_4\text{ yr}$ with $\tau_4 \approx 1.7$, so G343.1–2.3 should be safely in the Sedov phase with an expected angular size

$$\theta_{\text{SNR}} \approx 16'(E_{51}/n_0)^{1/5}t_4^{2/5}/d_3 \tag{1}$$

for a supernova releasing energy $E_0 = 10^{51}E_{51}\text{erg}$ in an external medium density $n_0\text{ cm}^{-3}$, at a true age 10^4t_4y at a distance $3d_3\text{ kpc}$. The observed size then implies $E_{51} \approx 11n_0t_4^{-2}d_3^5$, requiring a fairly energetic explosion for $d > 2\text{ kpc}$. During the Sedov phase the interior pressure is

$$P_{\text{SNR}} \approx 10^{-9}E_{51}^{2/5}n_0^{3/5}t_4^{-6/5}\text{g}/\text{cm}/\text{s}^2 \tag{2}$$

and is relatively constant away from the SNR limb.

The pulsar blows a wind bubble within this SNR interior, whose radius is $R_{\text{PWN}} \approx (E_*/E_0)^{1/3} R_{\text{SNR}}$ for a PWN bubble energy $E_* = f \dot{E} \tau_c$ (van der Swaluw & Wu 2001). Although the accuracy of this dependence of PWN radius on pulsar injection energy has been questioned (Blondin, Chevalier & Frierson 2001), we adopt it for the following estimates. With the observed ratio of radii, $R_{\text{PWN}}/R_{\text{SNR}} = 1.8'/25'$, we obtain $E_* = 3.7 \times 10^{-4} E_0$, i.e. this PWN has quite low internal energy. This is also reflected in the low radio and X-ray fluxes. Together we use these estimates, the observed size of the SNR, equation (1) and the measured $\dot{E}_{36} = 3.4$ and $\tau_c = 1.75 \times 10^4 \text{y}$ to write $f \approx (R_{\text{PWN}}/R_{\text{SNR}})^3 E_0 / (\dot{E} \tau_c) = 2.1 n_0 t_4^{-2} d_3^5$. Now, if the PWN is adiabatic and we assume spindown with constant B and braking index $n = 3$ from an initial period P_0 , we find that the total energy in the plerion is $[(P/P_0)^2 - 1] \dot{E} \tau_c$. Then, setting $f = (P/P_0)^2 - 1$ and eliminating the true age t using $t = \tau_c [1 - (P_0/P)^2]$ for magnetic dipole spindown, we obtain a constraint on the initial spin period

$$[1 - (P_0/P)^2]^3 / (P_0/P)^2 = 0.68 n_0 d_3^5 \quad (3)$$

which has a solution of $P_0 = 0.61P = 62 \text{ms}$ for $d=3 \text{kpc}$, and $P_0 = 0.79P = 80 \text{ms}$ for $d=2 \text{kpc}$. The corresponding true ages are $0.61\tau_c$ ($1.1 \times 10^4 \text{y}$) and $0.38\tau_c$ ($0.67 \times 10^4 \text{y}$), respectively. These numerical values are for $n_0 = 1$ and the density dependence from Equation (3) is quite weak. van der Swaluw & Wu (2001) present a similar sum for P_0 , assuming a known E_0 ; the above formulation emphasizes the sensitivity to the poorly known d . Note that with the large implied initial period, the integrated PWN energy is quite comparable to the present spin energy, with $f \approx 1.7$ at $d=3 \text{kpc}$ and $f \approx 0.62$ at $d=2 \text{kpc}$. So the spindown luminosity is roughly constant in the adiabatic phase and the PWN growth is closer to $t^{11/15}$ than to the $t^{3/10}$ law appropriate for impulsive energy injection (van der Swaluw 2001).

Inside this wind bubble, the Sedov interior pressure confines the PWN, giving rise to a termination shock at

$$\theta_{\text{WS}} \approx (\dot{E}/4\pi c P_{\text{SNR}})^{1/2} / d. \quad (4)$$

which results in $\theta_{\text{WS}} \approx 1''.2 \dot{E}_{36}^{1/2} E_{51}^{-1/5} n_0^{-3/10} t_4^{3/5} d_3^{-1}$. If we apply the SNR estimate for E_0 above, this becomes $\theta_{\text{WS}} \approx 0''.72 \dot{E}_{36}^{1/2} n_0^{-1/2} t_4 d_3^{-2}$. Then, using $\dot{E}_{36} \approx 4$ and applying the age estimate following Equation (3) we get $\theta_{\text{WS}} \approx 1''.5 n_0^{-1/2}$ ($d=3 \text{kpc}$) or $\theta_{\text{WS}} \approx 2''.1 n_0^{-1/2}$ ($d=2 \text{kpc}$). These estimates are reasonably consistent with the observed $3''$ torus radius, especially since an equatorially concentrated flow should have a stand-off distance $1.5\text{--}2 \times$ this spherical scale. The polar jets can have an initial shock at somewhat larger angle, with the resulting pitch angle scattering illuminating the jets somewhat further from the pulsar.

Of course, this bubble is offset from the center of G343.1–2.3 at $R = 0.5 R_{\text{SNR}}$ (figure 1). This is inside the $\sim 0.68 R_{\text{SNR}}$ where van der Swaluw, Downes & Keegan (2004) note that the increasing density causes the pulsar to be supersonic, so a bow shock should not have yet formed. These authors however compute numerical models of a fast moving pulsar in a SNR interior. As the pulsar moves, the PWN should become highly asymmetric with a ‘relic PWN’ at the SNR center and the pulsar placed near the leading edge of the PWN; see van der Swaluw, Downes & Keegan (2004) figures 7 and 8. We see no PWN structure near the geometric center of G343.1–2.3 and, if the ‘bubble nebula’ is identified with the shocked pulsar wind, the pulsar is certainly not offset from its center along the proper motion axis (away from the SNR center). So these models are an inadequate description of G343.1–2.3. From Figure 2, the pulsar is well centered in the bubble nebula, with any offset from its center along the axis to the SNR substantially less than $30\Delta_{30} \text{arcsec}$. Thus

$$v < 40\Delta_{30} d_3 / t_4 \text{ km/s}, \quad (5)$$

and the pulsar cannot have moved far from the explosion center. This is, of course, consistent with the scintillation results.

We can reconcile the symmetric PWN with the offset SNR shell if we assume that the pulsar progenitor exploded toward the edge of a quasi-spherical cavity. One scenario (also posited by Gvaramadze 2002, Bock & Gvaramadze 2002) that can associate the low velocity pulsar with G343.1–2.3 is to assume that the progenitor star had a stellar wind of mass loss rate $\dot{M}_{-8} 10^{-8} M_{\odot}/\text{yr}$ and wind speed $10^8 v_{w8}$ cm/s over $t \sim t_7 10^7 \text{y}$, typical of the $\sim 10 M_{\odot}$ stars that dominate the pulsar progenitors (Maeder 1981). This evacuates a stellar wind bubble of size

$$\theta_{SW} = 46' \left(\dot{M}_{-8} v_{w8}^2 / n_0 \right)^{1/5} t_7^{3/5} / d_3. \quad (6)$$

During the main sequence lifetime, the star moving at $10 v_6$ km/s travels $\sim 2^\circ v_6 t_7 / d_3$ and so it can easily traverse its wind bubble. Thus, one can imagine an off-center supernova in a nearly symmetric stellar wind bubble of radius $\sim 25'$: the supernova blast wave expands to fill the bubble, passing to the Sedov phase near its present radius. The supernova produces a neutron star with little or no kick, placing the pulsar near its present position. This has the added advantage of accommodating the rather large SNR size with a more modest energy of a few $\times 10^{51}$ erg. The PWN energy and size estimates above would then be somewhat amended; this would require a careful numerical simulation.

For the reasons detailed in the introduction, it is not yet clear that PSR B1706–44 and G343.1–2.3 are associated. So for completeness we can consider the case when the shocked pulsar wind blows an adiabatic bubble in a static, low P_{ext} external medium (Castor, McCray & Weaver 1975). If we assume that the pulsar was born (sans SNR) or entered a confining region of the ISM $\sim 10^4 \text{y}$ ago and that since then it has been spinning down at the present energy loss rate, we find that it will blow a bubble of angular size

$$\theta_{\text{BN}} \approx 0.76 (\dot{E} t^3 / \rho)^{1/5} / d \approx 120'' (\dot{E}_{36} / n_0)^{1/5} \tau_4^{3/5} / d_3. \quad (7)$$

These estimates change somewhat for a pulsar born at $P_0 \ll P$; since we are not making the association with the SNR G343.1–2.3, we can make no estimate of the initial spin period. As first noted by Dodson & Golap (2002), the $\sim 4'$ wide radio spur across the face of G343.1–2.3 has the approximate scale of such a ‘bubble nebula’. If the PWN stays unmixed (relativistic) then the interior of the bubble will have a pressure $P_{\text{BN}} \approx \dot{E} t / (4\pi R^3) \approx 1.6 \times 10^{-10} \left(n_0^3 \dot{E}_{36}^2 / \tau_4^4 \right)^{1/5}$ g/cm/s². In turn, the torus termination shock in this medium is at

$$\theta_{\text{WS}} \approx 2'9 (\dot{E}_{36} / n_0)^{3/10} \tau_4^{2/5} / d_3. \quad (8)$$

If (e.g. through Rayleigh-Taylor instabilities) the pulsar wind is well mixed with the swept up gas, the adiabatic thermal pressure would be $\sim 2 \times$ larger. Interestingly, the angular scales for this scenario are also reasonably compatible with the observed torus and bubble nebula size. Of course this scenario leaves open the question of the pulsar origin. Again the pulsar would need to have a quite low velocity to produced the observed symmetry.

Turning to the spectral results, we note that Possenti et al. (2002) fit a correlation between spindown energy and the PSR+PWN luminosity: $L(2 - 10 \text{keV}) = 1.8 \times 10^{38} \dot{E}_{40}^{1.34} \text{erg/s}$. For the PSR B1706–44 parameters this predicts a flux $f(2 - 10 \text{keV}) = 4.7 \times 10^{-12} d_3^{-2} \text{erg/cm}^2/\text{s}$. The observed 2-10 keV flux is in fact $\sim 1.7 \times 10^{-12} \text{erg/cm}^2/\text{s}$, even including the outer ‘bubble nebula’; without this component it is half as large. These correlations are not very accurate, but this does imply that the PSR B1706–44 PWN is substantially under-luminous for any distance less than 3 kpc. Gotthelf (2003) has derived correlations between the pulsar spindown power and the pulsar/PWN spectral indices. His relation predicts $\Gamma_{\text{PSR}} = 0.63 \pm 0.17$ (substantially smaller than our power law index $\sim 1.6 \pm 0.2$) and $\Gamma_{\text{PWN}} = 1.3 \pm 0.3$ (not inconsistent with the values measured for the torus and equatorial PWN).

As described in §2.4, the spectrum softens appreciably from the central torus to the outer bubble nebula. This suggests increased aging of the synchrotron population. Figures 2 and 3 show that the bulk of the radio emission lies in the ‘bubble nebula’ region. So we can take the radio flux and spectral index from Giacani et al. (2001) and compare with our nebula X-ray flux (Fig. 4). Comparing the radio spectral index $\alpha_R = 0.3$ with the best fit X-ray index $\alpha_X = 0.77$, shows a break quite close to the $\Delta\alpha = 0.5$ expected from synchrotron cooling. The extrapolated intersection of these power laws gives a break frequency of $\text{Log}[\nu_B(\text{Hz})] = 12.2_{-1.1}^{+0.9}$. For the fiducial pulsar age of $\sim 1.7 \times 10^4$ y, this corresponds to a nebula field of $1.4_{-0.6}^{+2.1} \times 10^{-4}$ G. Note that the magnetic pressure from this (photon flux-weighted) average field is $\sim 8 \times 10^{-10}$ g/cm², somewhat larger than the nebula pressure estimated from its radius. This may indicate field compression in the nebula limb. In general, if the mean nebula field is $10^{-4}B_{-4}$ G for a nebula of angular radius $\sim 100''\theta_{100}$, the total nebula field energy is $E_B \approx 1.5 \times 10^{47} B_{-4}^2 (\theta_{100} d_3)^3$ erg. This is comfortably less than the present spin energy $E_{\text{PSR}} \approx 2 \times 10^{48}$ erg, so the nebula can be easily powered even if the pulsar was born close to its present spin period. We find that this cooling break field is substantially larger than the equipartition field of $10 - 15 \mu\text{G}$ inferred for the radio and X-ray emitting populations (also the minimum equipartition nebula energy $\sim 9 \times 10^{45}$ erg is substantially smaller). The cooling break field can also be compared to that expected from simple radial evolution of the pulsar surface field: if this field $B_* = 3 \times 10^{12}$ G falls off as r^{-3} to the light cylinder, then as $1/r$ to the wind shock where it is compressed we get $B_{\text{WS}} \sim 3B_* r_*^3 / (r_{\text{LC}}^2 r_{\text{WS}}) \sim 1 \text{mG}$. If it continues to fall off as $1/r$ beyond this we get a field at the limb of the bubble nebula of $\sim 30 \mu\text{G}$. So the best we can do is to infer a mean nebular field $\sim 10 - 30 \times$ the equipartition value, with some generation of new field beyond the torus wind shock. The energetic requirements for this field, required to match the ν_B cooling break, are comfortably less than the energy available from PSR B1706–44. These field estimates are consistent with the non-detection of TeV ICS flux from this source (Aharonian et al. 2005).

The narrow outer jets also have a power-law spectrum and are almost certainly synchrotron-emitting. For a reasonable $0.1 B_{-4} \text{mG}$ field, the observed X-rays of $E_\gamma = 1.5 B_{-4} \Gamma_{7.5}^2$ keV require substantial e^\pm energies, with $\Gamma_e = 3 \times 10^7 \Gamma_{7.5}$ near the radiation-reaction limited primary Lorentz factor inferred for many polar cap (Muslimov & Harding 2003) and outer magnetosphere (Romani 1996) pulsar models. Since the jet is narrow, confinement of these pairs imposes a (not very restrictive) lower bound on the jet field $B_{-4} > 0.075 E_5^{1/3} / (d_3 \theta_w)$ where the maximum observed jet photon has $E \sim 5 E_5$ keV and the observed outer jet half-width is θ_w arcsec. A more restrictive upper limit on the mean jet field comes from the observation that the jets do not soften noticeably before their end $\sim 30 \theta_{30}$ arcsec from the pulsar. If we assume a jet bulk speed βc , then arguing that the flow time is shorter than the synchrotron cooling time gives us the limit $B_{-4} < 8.5 \left(\frac{\beta}{d_3 \theta_{30}} \right)^{2/3} E_5^{-1/3}$.

When the observed jet spectrum has an energy index of $\alpha = \Gamma - 1 \approx 0.3$, we infer a power-law spectrum of e^\pm in the jet $N(\Gamma_e) d\Gamma_e = K \Gamma_e^{-p} d\Gamma_e$, with $p = 2\alpha + 1 \approx 1.6$. We can then make an estimate of the minimum jet luminosity, i.e. at ‘equipartition’ when $B^2 = 6\pi m_e c^2 \int \Gamma_e N(\Gamma_e) d\Gamma_e$. Given the observed combined outer jet luminosity (0.5–8 keV) $L = 4\pi d^2 f_{\text{oj}} \approx 2.7 \times 10^{31}$ erg/s and emitting volume $V \approx 2 \times \theta_L \times \pi \theta_w d^3 \approx 1.1 \times 10^{52} (\theta_L/20) \theta_w^2 d_3^3$ cm³ with the angles in arcsec, we can estimate the equipartition field for an isotropic plasma as

$$B_{\text{eq}} = \left[\frac{18\pi}{\sigma_T} \left(\frac{2\pi m_e c}{E_{\text{max}}} \right)^{1/2} \frac{2(1-\alpha)}{1-2\alpha} \frac{1 - (E_{\text{min}}/E_{\text{max}})^{(1-2\alpha)/2}}{1 - (E_{\text{min}}/E_{\text{max}})^{(1-\alpha)}} \frac{L}{V} \right]^{2/7} \quad (9)$$

where the observed photon spectrum runs from E_{min} to E_{max} . For the observed flux this gives

$$B_{\text{eq}} \approx 0.25 \times 10^{-4} q(\alpha) [\theta_L \theta_w^2 d_3 / 20]^{-2/7} \text{ G}, \quad (10)$$

where $q(\alpha = 0.3) = 1$ is a weak function of α . The corresponding minimum energy flux for the outer jet is

$$L_{\text{oj}} = 8 \times 10^{33} \beta d_3^{12/7} \theta_w^{10/7} (\theta_L/20)^{-2/7} \text{erg/s}, \quad (11)$$

where the jet bulk velocity is βc . This is $\sim 10^{-3} \dot{E}$ per jet and will, of course, be larger if the jet flow includes ions. Interestingly, if the pulsar couples roughly isotropically to the PWN, then the corresponding fraction of the outflow should subtend a half angle of $\sim 5^\circ$. This is somewhat smaller than the angle subtended by the inner jets, but $\sim 3\times$ larger than the $\sim 1''$ width of the ends of the jet – there is substantial collimation of the jet energy flux.

We have argued that a low PSR velocity can explain the symmetry of the PWN. The central location of the pulsar and spherical post-shock flow may also allow the equatorial toroidal structure and polar jets to propagate undisturbed to large radii. We do, however, measure a small misalignment of the outer jets, corresponding to a deflection of $\theta_{\text{de}} = 1.3 \pm 0.15^\circ$ for each. If we imagine a pressure acting along the jet’s $\sim 30''$ length, then the required perturbation is $\delta P \approx L_{\text{oj}} \tan \theta_{\text{de}} / (\beta c A_{\text{oj}}) \approx 5 \times 10^{-14} L_{34} / (\beta \theta_{30} \theta_w d_3^2) \text{g/cm}^2$, where A_{oj} is the jet’s cross sectional area. This is only $\sim 10^{-3}$ of the total pressure in the nebula. It could be due to ram pressure if the shocked nebular medium flows to the west at $v \sim 1.7 n_{\text{neb}}^{-1/2} \text{km/s}$.

Our X-ray measurements have established the PWN symmetry axis, presumably reflecting the pulsar

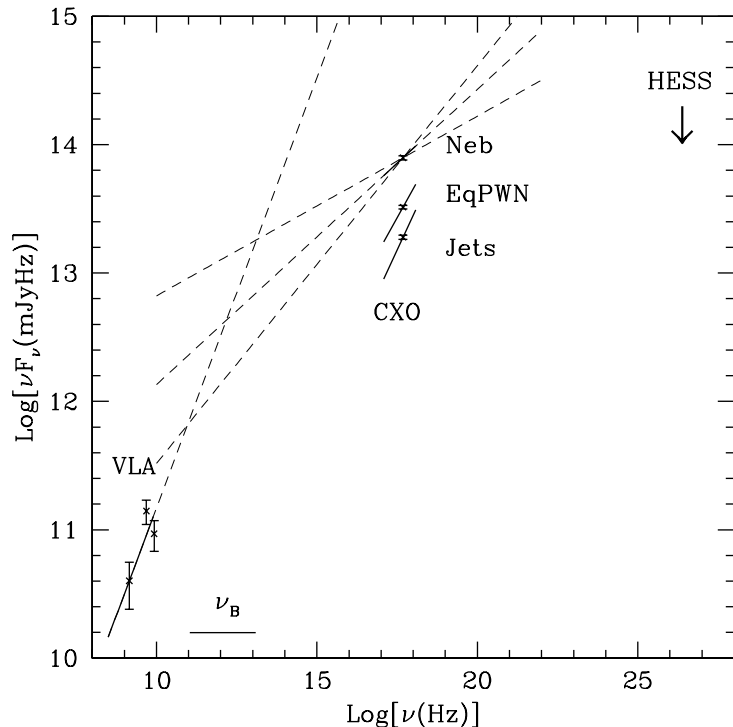


Fig. 4.— Outer PWN (‘bubble nebula’) spectral energy distribution (SED). Radio data are from Giacani et al. (2001), the TeV upper limit is from Aharonian et al. (2005). The spectra of the inner, younger PWN components are plotted for comparison. The extension of the radio PL and the best fit nebula (outer PWN) PL meet at $\nu_B \sim 1.6 \times 10^{12} \text{Hz}$; the indices are consistent with a $\Delta\alpha = 0.5$ cooling break.

spin axis, to very high precision. Unfortunately our original goal of relating this to the proper motion axis remains unfulfilled. It is true that the torus symmetry axis points roughly toward the center of G343.1–2.3, confirming the estimates from earlier *Chandra* data. However, the PWN symmetry about the pulsar and the low scintillation velocity suggest a very low transverse speed $\leq 40\text{km/s}$, which would preclude a birth site as distant as the SNR center. This low speed makes a direct proper motion challenging, but allows latitudinal asymmetries in the PWN flow to propagate undisturbed to fairly large radius, where they can be imaged with *Chandra*. Thus, study of this PWN offers some good opportunities to probe outflow dynamics and jet collimation. Study of this, and similar, PWNe may prove useful electrodynamic analogs of the $10^6\times$ more powerful AGN jets. A viable scenario for maintaining the G343.1–2.3/PSR B1706–44 association posits a supernova event near the present pulsar site, with the remnant inflating a pre-existing off-center cavity. However, the residual (small) proper motion could then have any direction. In fact, the faint extension of the PWN (bubble nebula) to the west and the increased radio surface brightness to the east might suggest a rather slow pulsar motion at $\text{PA} \sim 80^\circ$. This would be nearly orthogonal to the torus symmetry axis. With the large P_0 estimated here, this could be construed as suggesting poor rotational averaging of a birth kick (Ng & Romani 2004). So the PWN/SNR geometry offers both aligned and orthogonal axes. Only a sensitive astrometric campaign can detect or limit the pulsar motion and resolve this ambiguity.

This work was supported in part by NASA grants SAO G04-5060X and NAG5-13344. We thank the referee for several careful readings, which resulted in substantial changes. We also thank R.N. Manchester who provided a current pulsar ephemeris for the VLBI experiment.

REFERENCES

- Aharonian, F. et al 2005, *A&A*, 432, L9
- Bock, D.C.-J. & Gvaramadze, V.V. 2002, *A&A*, 394, 533
- Blondin, J.M., Chevalier, R.A. & Frierson, D.M. 2001, *ApJ*, 563, 806
- Castor, J., McCray, R. & Weaver, R. 1975, *ApJ*, 200, L107
- Chadwick, P.M. et al 1997, in *Proc. 26th Cos Ray Conf*, 3, 189
- Chevalier, R.A. 2005, *ApJ*, 619, 839
- Cordes, J.M. & Lazio, T.J.W. 2002, *astro-ph/0207156*
- Dodson, R. & Golap, K. 2002, *MNRAS*, 334, L1
- Dodson, R., Lewis, D., McConnell, D. & Deshpande, A.A. 2003, *MNRAS*, 343, 116
- Frater, R.H., Brooks, J.W., & Whiteoak, J.B. 1992, *JEEE*, 12, 103
- Giacani, E.B., Frail, D.A., Goss, W.M. & Vietes, M. 2001, *AJ*, 121, 3133
- Gotthelf, E.V. 2003, *ApJ*, 591, 361
- Gotthelf, E., Halpern, J.P. & Dodson, R. 2002, *ApJL*, 567, L125
- Gvaramadze, V.V. 2002, in *Neutron Stars in Supernova Remnants*, ed. P. O. Slane, & B. M. Gaensler (San Francisco: ASP), *ASP Conf. Ser.*, 271, 23

- Johnston, S. et al 1992, MNRAS, 255, 401
- Johnston, S., Nicastro, L., Koribalski, B. 1998, MNRAS, 297, 108
- Kifune, T. et al. 1995, ApJ, 438, L91
- Koribalski, B., Johnston, S., Wiesberg, J., Wilson, W. 1995, ApJ, 441, 756
- Lai, D., Chernoff, D.F. & Cordes, J.M. 2001, ApJ, 549, 1111
- Maeder, A. 1981, AA, 102, 401
- McAdam, W., Osborne, J & Parkinson, M. 1993, *Nature*, 361, 516
- McGowan, K.E. et al 2004, ApJ, 600, 343
- Mori, K. et al 2001, ASPC, 251, 576
- Muslimov, A. & Harding, A.K. 2003, ApJ, 588, 430
- Ng, C.-Y. & Romani, R.W. 2004, ApJ, 601, 479
- Nicastro, L., Johnston, S. & Koribalski, B. 1996, AA, 306, L49
- Pavlov, G.G., Teter, M.A., Kargaltsev, O. & Sanwal, D., 2003, ApJ, 591, 1157
- Possenti, A. 2003, AA, 387, 993
- Rees, M.J. & Gunn. J.E. 1974, MNRAS, 167, 1
- Romani, R.W. & Yadigaroglu, I.-A. 1995, ApJ, 438, 314.
- Romani, R.W. 1996, ApJ, 470, 469
- Romani, R.W. 2004, Proc Ast. Soc. Pac., 328; astro-ph/0404100
- Spruit, H. & Phinney, E.S. 1998, *Nature*, 393, 139
- van der Swaluw, E., Achterberg, A., Gallant, Y.A., Toth, G. 2001 A&A, 380, 309
- van der Swaluw, E., Downes, T.P & Keegan, R. 2004, A&A, 420 937
- van der Swaluw, E. & Wu, Y. 2001, ApJ, 555, L49
- Zavlin, V.E. et al 1996, AA, 315, 141